

Characterization of the convective instability of the Aw-Rascle-Zhang model via spectral analysis

Francois Belletti^a

Mandy Huo^b

Xavier Litrico^c

Alexandre M. Bayen^{a, d}

Abstract—This article starts from the classical Aw-Rascle-Zhang (ARZ) model for freeway traffic and develops a spectral analysis of its linearized version. A counterpart to the Froude number in hydrodynamics is defined that enables a classification of the nature of vehicle traffic flow using the explicit solution resulting from the analysis. We prove that our linearization about an equilibrium is stable for congested regimes and convective-unstable otherwise. NGSIM data for congested traffic trajectories is used to compare the linearized model’s predictions with actual macroscopic behavior of traffic. The model is shown to achieve good accuracy for speed and flow. In particular, it replicates the propagation of boundary conditions’ oscillations into the interior resolution domain of the PDE under study.

I. INTRODUCTION

Researchers aiming at devising control strategies for road traffic face a trade-off between empirical evidence confirming the accuracy of non-linear models [1], [2] and the ease of use of linear systems when it comes to designing controllers.

Non-linear second order models such as Payne-Whitham [3], [4] were first presented as a compelling alternative to first order models [5], [6] that accounted for many features observed empirically in traffic such as stop-and-go behavior. Although Daganzo highlighted many flaws of the first generation of that family of models [7], a second generation including the Aw-Rascle equations [8] and phase transition models [9] offered a step towards more realism in macroscopic traffic modeling.

The Aw-Rascle-Zhang model – one of the most accurate in that group [10] – accounts for persisting oscillations, information propagation anisotropy and drivers’ impulse to shorten their travel times. Linearizing the ARZ model, based on the work of Litrico and Fromion [11] for the Saint-Venant equations, offers a unique opportunity to work in a realistic modeling framework where the phenomena mentioned above are accounted for and, at the same time, use linear control theory and spectral Laplace analysis.

Our approach in this article is therefore to linearize the ARZ model about an equilibrium so as to make the best of a trade-off between model accuracy and ease of use. The first section is dedicated to the linearization and spectral analysis

of the ARZ model. We prove convective instability in free-flow regime that drives the model away from its equilibrium state and devise an equivalent of the hydrodynamics’ Froude number for traffic macroscopic models. Laplace transforms and low frequency analysis also enable a tractable interpretation of the underlying dynamics of the system which we present. After having introduced the model in section II, section III proceeds with a spectral analysis of the linearized equations whose accuracy is empirically assessed in section IV. Their predictions are compared with ground truth data extracted from the NGSIM data set for the US-101 freeway.

II. THE ARZ MODEL

We consider the ARZ model with relaxation term.

$$\rho_t + (\rho v)_x = 0, \quad (1)$$

$$(v - V(\rho))_t + v(v - V(\rho))_x = \frac{V(\rho) - v}{\tau}, \quad (2)$$

where ρ is the density, v is the velocity, τ is the relaxation time, and $V(\rho) = Q(\rho)/\rho$ is the equilibrium velocity profile. Finally $Q(\rho)$ is the density-flow relation given by the fundamental diagram. We assume that V is C^1 derivable over its domain.

In vector form the ARZ model is

$$\begin{pmatrix} \rho \\ v \end{pmatrix}_t + \begin{pmatrix} v & \rho \\ 0 & v + \rho V'(\rho) \end{pmatrix} \begin{pmatrix} \rho \\ v \end{pmatrix}_x = \begin{pmatrix} 0 \\ V(\rho) - v \end{pmatrix} \quad (3)$$

With the appropriate change of variable, we can rewrite the model in the density-flow and velocity-flow forms, the latter of which is most useful to us for practical control purposes. Using the flow relation $q = \rho v$ and (3), the speed-flow form is

$$\begin{pmatrix} v \\ q \end{pmatrix}_t + C(v, q) \begin{pmatrix} v \\ q \end{pmatrix}_x = \frac{1}{\tau} \begin{pmatrix} V\left(\frac{q}{v}\right) - v \\ Q\left(\frac{q}{v}\right) - q \end{pmatrix}, \quad (4a)$$

$$C(v, q) = \begin{pmatrix} v + \frac{q}{v} V'\left(\frac{q}{v}\right) & 0 \\ \frac{q}{v} & v + \frac{q}{v} V'\left(\frac{q}{v}\right) \end{pmatrix}. \quad (4b)$$

The (v, q) form has seldom been used in transportation engineering however it is promising for data fusion purposes that involve both loop detector measurements (providing values for q) and GPS traces (giving estimates for v).

A. Linearization

We are interested in small deviations, $(\tilde{\rho}(x, t), \tilde{v}(x, t))$, from a given nominal profile. Consider the nominal solution $(\rho^*(x), v^*(x))(V(\rho^*) = v^*)$ satisfying $v_t = \rho_t = 0$.

^aDepartment of Electrical Engineering and Computer Science, University of California, Berkeley, United-States, francois.belletti@berkeley.edu

^bDepartment of Physics, University of California, Berkeley, United-States

^cLyRE, R&D center of Lyonnaise des Eaux, 91, rue Paulin, 33029 Bordeaux cedex, France

^dDepartment of Civil and Environmental Engineering, University of California, Berkeley, United-States

Then (3) becomes

$$v^* \rho_x^* + v_x^* \rho^* = 0, \quad (5)$$

$$(v^* + \rho^* V'(\rho^*)) v_x^* = \frac{V(\rho^*) - v^*}{\tau} = 0. \quad (6)$$

Therefore we must have $v_x^* = \rho_x^* = 0$, so the solution is uniform along the road.

Linearization about the equilibrium $(\rho^* V(\rho^*) = q^*)$ with deviations $(\tilde{\rho}(x, t), \tilde{q}(x, t))$ gives the form in (7). It is most adapted to traffic prediction and control in practical settings where flows and vehicle velocities are measured. The following will derive explicit solutions to these equations.

$$\begin{pmatrix} \tilde{v} \\ \tilde{q} \end{pmatrix}_t + \bar{C} \begin{pmatrix} \tilde{v} \\ \tilde{q} \end{pmatrix}_x = \bar{B} \begin{pmatrix} \tilde{v} \\ \tilde{q} \end{pmatrix}, \quad (7a)$$

$$\bar{C} = \begin{pmatrix} v^* + \frac{q^*}{v^*} V'(\frac{q^*}{v^*}) & 0 \\ \frac{q^*}{v^*} (v^* + \frac{q^*}{v^*} V'(\frac{q^*}{v^*})) & v^* \end{pmatrix} \quad (7b)$$

$$\bar{B} = \frac{1}{v^* \tau} \begin{pmatrix} -\frac{(v^*)^2 + q^* V'(\frac{q^*}{v^*})}{v^*} & V'(\frac{q^*}{v^*}) \\ -\frac{q^* ((v^*)^2 + q^* V'(\frac{q^*}{v^*}))}{(v^*)^2} & \frac{q^* V'(\frac{q^*}{v^*})}{v^*} \end{pmatrix} \quad (7c)$$

B. Characteristic form

Diagonalization of the velocity-flow yields

$$\begin{pmatrix} \xi_1 \\ \xi_2 \end{pmatrix}_t + \underbrace{\begin{pmatrix} \lambda_1 & 0 \\ 0 & \lambda_2 \end{pmatrix}}_A \begin{pmatrix} \xi_1 \\ \xi_2 \end{pmatrix}_x = \underbrace{\begin{pmatrix} -\frac{1}{\tau} & 0 \\ -\frac{1}{\tau} & 0 \end{pmatrix}}_B \begin{pmatrix} \xi_1 \\ \xi_2 \end{pmatrix}, \quad (8)$$

where the eigenvalues, $\lambda_1 = v^*$ and $\lambda_2 = v^* + \frac{q^*}{v^*} V'(\frac{q^*}{v^*})$, $\xi_1 = \frac{\rho^* \lambda_2}{\lambda_1 - \lambda_2} \tilde{v} + \tilde{q}$ and $\xi_2 = \frac{q^*}{\lambda_1 - \lambda_2} \tilde{v}$. Assuming $V'(\rho^*) \neq 0$, this is consistent with the physical dynamics of the system as no waves travel faster than the equilibrium vehicle speed.

C. The Traffic Froude Number

In fluid mechanics, the Froude number is a dimensionless number which delineates the boundary between flow regimes [11], [12]. Using the eigenvalues of the system in the characteristic form, we are able to define a useful counterpart to this number. With the assumptions above on V' , there are two flow regimes: one in which $\lambda_1 \lambda_2 < 0$ and one characteristic line travels downstream whereas the other characteristic line travels upstream, and one in which $\lambda_1 \lambda_2 > 0$ and both characteristic lines travel downstream. We define the *Traffic Froude Number* (TFN) as

$$F = \left| \frac{\rho^* V'(\rho^*)}{v^*} \right|. \quad (9)$$

Then we have

$$\begin{cases} F > 1 & \Rightarrow |\rho^* V'(\rho^*)| > v^* & \Rightarrow \lambda_2 < 0 \\ F < 1 & \Rightarrow |\rho^* V'(\rho^*)| < v^* & \Rightarrow \lambda_2 > 0 \end{cases}$$

Hence the system is in free-flow when $F < 1$ and congestion when $F > 1$. In hydrodynamics these regimes are respectively named subcritical and supercritical [11]. The direction

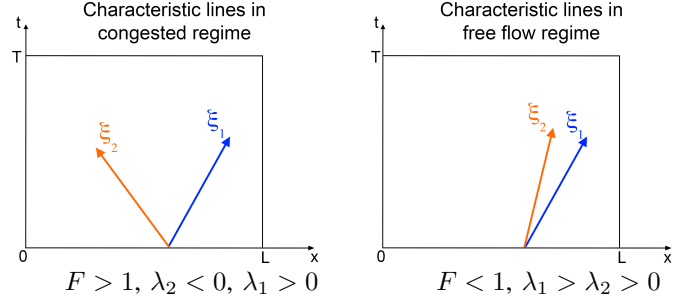


Fig. 1. Illustration of characteristic lines in congested (supercritical) and free-flow regime (subcritical) ξ_1 and ξ_2 propagate along.

of characteristic lines is illustrated in Figure 1. Note also that $\lambda_2 = v^* + \rho^* V'(\rho^*) = \frac{Q(\rho^*)}{\rho^*} + \frac{\rho^* Q'(\rho^*) - Q(\rho^*)}{\rho^*} = Q'(\rho^*)$.

For traffic, the interpretation of the different regimes is somewhat different. Free flow regime corresponds to light traffic in which drivers go as fast as the desired speed. The congested regime arises when traffic is denser and, because too many cars are present on the same freeway section, drivers slow down and eventually form traffic jam.

III. SPECTRAL ANALYSIS OF THE LINEARIZED ARZ MODEL

We now consider the (v, q) system for the frequency domain analysis for practical control purposes.

A. State-transition matrix

Taking the Laplace transform of the diagonalized form (8) we obtain $\frac{\partial \hat{\xi}(x, s)}{\partial x} = \mathcal{A}(s) \hat{\xi}(x, s) + \mathcal{B} \xi(x, t = 0^-)$ where $\mathcal{A}(s) = A^{-1}(B - sI)$ and $\mathcal{B} = -A^{-1}$. Assuming zero initial conditions we have $\hat{\xi}(x, s) = \Phi(x, s) \hat{\xi}(0, s)$ where $\Phi(x, s) = e^{\mathcal{A}(s)x}$ is the state-transition matrix.

To compute the exponential we diagonalize the matrix $\mathcal{A}(s)$ which then yields the components of $\Phi(x, s)$:

$$\phi_{11}(x, s) = e^{-\frac{x}{\tau \lambda_1}} e^{-\frac{x}{\lambda_1} s}, \quad (10a)$$

$$\phi_{12}(x, s) = 0, \quad (10b)$$

$$\phi_{21}(x, s) = \frac{\lambda_1 \left(e^{-\frac{x}{\tau \lambda_1}} e^{-\frac{x}{\lambda_1} s} - e^{-\frac{x}{\lambda_2} s} \right)}{\lambda_2 - \tau(\lambda_1 - \lambda_2)s}, \quad (10c)$$

$$\phi_{22}(x, s) = e^{-\frac{x}{\lambda_2} s}. \quad (10d)$$

B. Free-flow case ($F < 1$)

Consider the system in the free-flow regime. With $\xi_1(0, t)$ and $\xi_2(0, t)$ as the inputs and $\xi_1(L, t)$ and $\xi_2(L, t)$ as the outputs, the distributed transfer matrix is exactly the state-transition matrix $\Phi(x, s)$. Inverting the linear transform that gives ξ_1 and ξ_2 as functions of v and q , we can write

$$\frac{\begin{pmatrix} \tilde{v}(x, s) \\ \tilde{q}(x, s) \end{pmatrix}}{\lambda_2} = \Psi(x, s) \begin{pmatrix} \tilde{v}(0, s) \\ \tilde{q}(0, s) \end{pmatrix} \quad \text{where, letting } \alpha =$$

$$\psi_{11}(x, s) = \frac{\alpha e^{-\frac{x}{\lambda_1}(s+\frac{1}{\tau})} + s e^{-\frac{s x}{\lambda_2}}}{s + \alpha}, \quad (11a)$$

$$\psi_{12}(x, s) = \frac{1}{\rho^* \tau} \frac{e^{-\frac{s x}{\lambda_2}} - e^{-\frac{x}{\lambda_1}(s+\frac{1}{\tau})}}{s + \alpha}, \quad (11b)$$

$$\psi_{21}(x, s) = -s \rho^* \tau \alpha \frac{e^{-\frac{s x}{\lambda_2}} - e^{-\frac{x}{\lambda_1}(s+\frac{1}{\tau})}}{s + \alpha}, \quad (11c)$$

$$\psi_{22}(x, s) = \frac{s e^{-\frac{x}{\lambda_1}(s+\frac{1}{\tau})} + \alpha e^{-\frac{s x}{\lambda_2}}}{s + \alpha}. \quad (11d)$$

We have $\frac{1}{\lambda_1}(-\alpha + \frac{1}{\tau}) = \frac{-\alpha}{\lambda_2}$, thus a Taylor expansion about $-\alpha$ shows that numerators and denominators cancel out for $s \rightarrow -\alpha$, proving that the output remains bounded for a given value of x . We will show below that a conic region of the $[0, T] \times [0, L]$ domain features exponential growth in free-flow regime. This arises when changing t and x simultaneously and complements the conclusion formulated above.

1) *Low-frequency approximation for physical variables in free-flow regime:* To simplify the analysis of (11), we assume $|s| \ll |\alpha|$ which corresponds to traffic flow varying slowly and smoothly.

We find the following approximations:

$$\psi_{11}(x, s) \simeq e^{-\frac{s x}{\lambda_2}} e^{-\frac{x}{\tau \lambda_1}}, \quad (12a)$$

$$\psi_{12}(x, s) \simeq \frac{1}{\rho^* \tau \alpha} e^{-\frac{s x}{\lambda_2}} \left(1 - e^{-\frac{x}{\tau \lambda_1}}\right), \quad (12b)$$

$$\psi_{21}(x, s) \simeq -s \rho^* \tau e^{-\frac{s x}{\lambda_2}} \left(1 - e^{-\frac{x}{\tau \lambda_1}}\right), \quad (12c)$$

$$\psi_{22}(x, s) \simeq e^{-\frac{s x}{\lambda_2}}. \quad (12d)$$

Interpreting the low frequency expressions is fairly straightforward in terms of distributed delays featuring λ_1 or λ_2 as information propagation speeds and distributed gains where $\lambda_1 \tau$ is the characteristic damping distance. It is also remarkable that $\tilde{q}(x, s)$ appears as the result of a derivator applied to $\tilde{v}(0, s)$.

2) *Bode plots for free-flow regime:* We generate Bode plots using the following parameters taken from [13]: $q_{\max} = 1300$ veh/h, $\rho_{\max} = 0.1$ veh/m, and $L = 100$ m. The Greenshields fundamental diagram, $Q(\rho) = 4 \frac{q_{\max}}{\rho_{\max}} \rho (\rho_{\max} - \rho)$, is used to approximate the fundamental diagram. For inhomogeneous second-order models, the relaxation time, τ , falls in the range of about 14-60 seconds [10]. A relaxation time of $\tau = 15$ s is used for the following simulations. We simulate for $\rho^* = 0.01$ veh/m. Here the characteristic frequency of the system, $|\alpha|$, equals 0.53 Hz which is indeed sensible for traffic flow modeling.

The Bode plots for the physical variables are displayed in Figure 2.

For transfer functions with $1 - e^{-\frac{x}{\lambda_1 \tau \alpha}(s+\alpha)}$ as a factor (that is to say ψ_{12} and ψ_{21}) we observe in

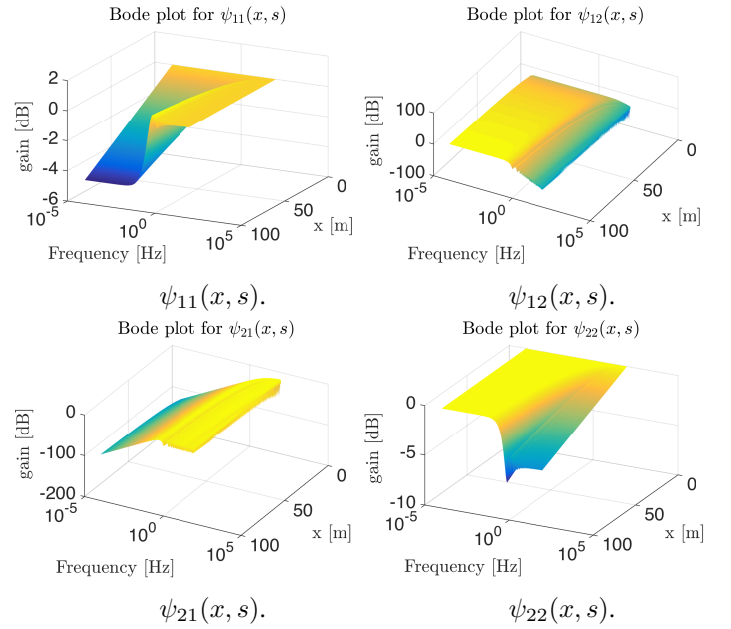


Fig. 2. Spatial magnitude Bode plots for physical variables in free-flow regime ($|\alpha| = 0.53$ Hz)

corresponding Bode plots that the value of the log-gain in high frequency tends to vary very sharply. Indeed, with $s = jw$, we have $\left|1 - e^{-\frac{x}{\lambda_1 \tau \alpha}(s+\alpha)}\right| = e^{-\frac{x}{\lambda_1 \tau} \sqrt{\left(e^{\frac{x}{\lambda_1 \tau}} - \cos\left(\frac{w}{\lambda_1 \tau \alpha} x\right)\right)^2 + \sin^2\left(\frac{w}{\lambda_1 \tau \alpha} x\right)}}$. Therefore, if the spatial pseudo-period $\tilde{L} = \frac{2\pi}{w} \lambda_1 \tau |\alpha|$ is low enough, near zero values appear when x is a multiple of \tilde{L} . This explains the irregular shape of the distributed Bode plots of ϕ_{21} , ψ_{12} , and ψ_{21} for frequencies $w \gg 2\pi \frac{\lambda_1 \tau |\alpha|}{L} = 6.53$ Hz. This does not impact the stability of the system. Bode plots only look irregular about such points because of the logarithmic scale.

3) *Step responses:* We analyze the behavior of the system given step inputs $\tilde{v}(0, t) = \bar{v}H(t)$ and $\tilde{q}(0, t) = \bar{q}H(t)$, where $H(\cdot)$ is the Heaviside function. The step responses can be explicitly computed from the spectral responses. Letting $H_1(t, x) = H\left(t - \frac{x}{\lambda_1}\right)$ and $H_2(t, x) = H\left(t - \frac{x}{\lambda_2}\right)$:

$$\begin{aligned} \tilde{v}(x, t) &= \bar{v} e^{-\frac{x}{\lambda_1 \tau}} H_1(t, x) \\ &+ \bar{v} e^{-\alpha\left(t - \frac{x}{\lambda_2}\right)} (H_2 - H_1)(t, x) \\ &- \frac{\bar{q}}{\rho^* \tau} \left(e^{-\frac{x}{\lambda_1 \tau}} H_1(t, x) - H_2(t, x) \right) \\ &- \frac{\bar{q}}{\rho^* \tau} e^{-\alpha\left(t - \frac{x}{\lambda_2}\right)} (H_2 - H_1)(t, x) \end{aligned} \quad (13)$$

$$\begin{aligned} \tilde{q}(x, t) &= \bar{v} \rho^* \tau \alpha e^{-\alpha\left(t - \frac{x}{\lambda_2}\right)} (H_1 - H_2)(t, x) \\ &+ \bar{q} H_2(t, x) \\ &+ \bar{q} e^{-\alpha\left(t - \frac{x}{\lambda_2}\right)} (H_1 - H_2)(t, x) \end{aligned} \quad (14)$$

In free-flow regime, because $\alpha < 0$, this set of time domain expressions reveal that within a cone marked by the characteristic lines, speed and flow linearization errors grow exponentially. This is consistent with the observations

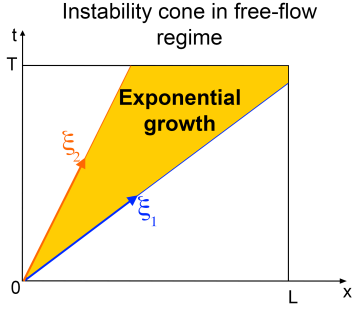


Fig. 3. Exponential growth cone appearing in the free-flow regime for v and q .

in [14] where small local perturbations occurring in free-flow regime can cause traffic to transition durably to the congested regime.

C. Congested regime ($F > 1$)

For the system in the congested regime, following (III-A) we can write $\begin{pmatrix} \hat{\xi}_1(x, s) \\ \hat{\xi}_2(x, s) \end{pmatrix} = \Gamma(x, s) \begin{pmatrix} \hat{\xi}_1(0, s) \\ \hat{\xi}_2(L, s) \end{pmatrix}$ with

$$\gamma_{11}(x, s) = e^{-\frac{x}{\lambda_1}(s + \frac{1}{\tau})}, \quad (15a)$$

$$\gamma_{12}(x, s) = 0, \quad (15b)$$

$$\gamma_{21}(x, s) = \frac{\lambda_1 \alpha e^{-\frac{x}{\lambda_1}(s + \frac{1}{\tau})}}{\lambda_2 (s + \alpha)} \left(1 - e^{-\frac{(L-x)}{\lambda_1 \tau \alpha}(s + \alpha)} \right), \quad (15c)$$

$$\gamma_{22}(x, s) = e^{\frac{s(L-x)}{\lambda_2}}. \quad (15d)$$

1) *Transfer functions for physical variables in congested regime:* In the congested regime, the boundary conditions determining the system are $\hat{\xi}_1(0, \cdot)$ and $\hat{\xi}_2(0, \cdot)$. By linearity of the Laplace transform $\hat{\xi}_1(0, s) = \frac{\rho^* \lambda_2}{\lambda_1 - \lambda_2} \hat{v}(0, s) + \hat{q}(0, s)$. Therefore, as $\hat{\xi}_2(0, s) = \gamma_{21}(0, s) \hat{\xi}_1(0, s) + \gamma_{22}(0, s) \hat{\xi}_2(L, s)$, we get $\hat{\xi}_1(0, s) = \frac{1}{d(s)} \hat{q}(0, s) + \frac{n(s)}{d(s)} \hat{v}(L, s)$ where $d(s) = 1 - \frac{\lambda_2}{\lambda_1} \gamma_{21}(0, s)$ and $n(s) = \frac{\rho^* \lambda_2}{\lambda_1 - \lambda_2} \gamma_{22}(0, s)$. The (v, q) system has only two degrees of freedom. Therefore we consider that the only inputs to the system are $q(0, \cdot)$ and $v(L, \cdot)$. At the boundary, $v(0, \cdot)$ is then completely determined and can be interpreted as an output of the system.

The corresponding transfer equation is

$$\begin{pmatrix} \hat{v}(x, s) \\ \hat{q}(x, s) \end{pmatrix} = \underbrace{R^{-1} \Gamma(x, s)}_{\Theta(x, s)} \begin{pmatrix} \frac{n(s)}{d(s)} & \frac{1}{d(s)} \\ \frac{\rho^* \lambda_2}{\lambda_1 - \lambda_2} & 0 \end{pmatrix} \begin{pmatrix} \hat{v}(L, s) \\ \hat{q}(0, s) \end{pmatrix} \quad (16)$$

where

$$\theta_{11}(x, s) = \frac{\alpha e^{-\frac{x}{\tau \lambda_1}} e^{-\frac{s}{\lambda_1}(x - L \frac{\lambda_1}{\lambda_2})} + s e^{-\frac{s}{\lambda_2}(x - L)}}{s + \alpha e^{-\frac{x}{\tau \lambda_1}} e^{-\frac{sL}{\lambda_1}(1 - \frac{\lambda_1}{\lambda_2})}}, \quad (17a)$$

$$\theta_{12}(x, s) = \frac{e^{-\frac{x}{\tau \lambda_1}} e^{-\frac{s}{\lambda_2}(x - L(1 - \frac{\lambda_2}{\lambda_1}))} - e^{-\frac{x}{\tau \lambda_1}} e^{-\frac{sx}{\lambda_1}}}{\rho^* \tau \left(s + \alpha e^{-\frac{x}{\tau \lambda_1}} e^{-\frac{sL}{\lambda_1}(1 - \frac{\lambda_1}{\lambda_2})} \right)}, \quad (17b)$$

$$\theta_{21}(x, s) = \rho^* \tau \alpha s \frac{e^{-\frac{s(x-L)}{\lambda_2}} - e^{-\frac{x}{\tau \lambda_1}} e^{-\frac{s}{\lambda_1}(x - L \frac{\lambda_1}{\lambda_2})}}{s + \alpha e^{-\frac{x}{\tau \lambda_1}} e^{-\frac{sL}{\lambda_1}(1 - \frac{\lambda_1}{\lambda_2})}}, \quad (17c)$$

$$\theta_{22}(x, s) = \frac{\alpha e^{-\frac{x}{\tau \lambda_1}} e^{-\frac{s}{\lambda_2}(x - L(1 - \frac{\lambda_2}{\lambda_1}))} + s e^{-\frac{x}{\tau \lambda_1}} e^{-\frac{sx}{\lambda_1}}}{s + \alpha e^{-\frac{x}{\tau \lambda_1}} e^{-\frac{sL}{\lambda_1}(1 - \frac{\lambda_1}{\lambda_2})}}. \quad (17d)$$

2) *Low-frequency approximation for physical variables in congested regime:* We derive approximate expressions in the frequency domain for the transfer functions above when $|s| \ll |\alpha|$:

$$\theta_{11}(x, s) \simeq e^{\frac{s(L-x)}{\lambda_2}} e^{\frac{L-x}{\tau \lambda_1}}, \quad (18a)$$

$$\theta_{12}(x, s) \simeq \frac{1}{\rho^* \tau \alpha} e^{-\frac{sx}{\lambda_1}} \left(1 - e^{\frac{L-x}{\tau \lambda_1}} \right), \quad (18b)$$

$$\theta_{21}(x, s) \simeq s \rho^* \tau e^{\frac{s(L-x)}{\lambda_2}} e^{\frac{L}{\tau \lambda_1}} \left(1 - e^{-\frac{x}{\tau \lambda_1}} \right), \quad (18c)$$

$$\theta_{22}(x, s) \simeq e^{-\frac{sx}{\lambda_1}}. \quad (18d)$$

With such expressions, interpreting the approximate transfer functions in low frequencies becomes fairly easy in terms of information propagating from the boundary conditions into the resolution domain with two different speeds: λ_1 and λ_2 . Once again we see distributed gain components with characteristic distance $\lambda_1 \tau$. A derivator component in θ_{21} relates $\hat{\xi}_2(x, s)$ to $\hat{\xi}_1(0, s)$.

3) *Bode plots for congested regime:* We use the same fundamental diagram as in the free-flow case. However the linearization point, $\rho^* = 0.08$ veh/m, corresponds to the congested region of the Greenshields diagram. We show the distributed Bode plots for the physical variables in Figure 4. In that case, $\alpha = 0.05$ Hz, which does correspond to a reasonable characteristic frequency for traffic modeling applications.

Similarly to the free-flow case, for high frequencies ($w \gg 2\pi \frac{\lambda_1 \tau \alpha}{L} = 0.13$ Hz) near zero values appearing with spatial periodicity $\frac{2\pi}{w} \lambda_1 \tau \alpha$ almost cancel out γ_{21} , θ_{12} , and θ_{21} . Such points only appear as irregularities in the Bode plots because the gain is computed on a logarithmic scale.

Gain and phase margins are not discussed here in the interest of concision.

4) *Poles and BIBO stability of the system:* A numerical search for roots of the denominator of the transfer functions conducted using standard equation solvers found poles at $-\alpha$ and $s = -0.0018$. Both are negative reals and therefore cannot make the system unstable. Although the solvers could

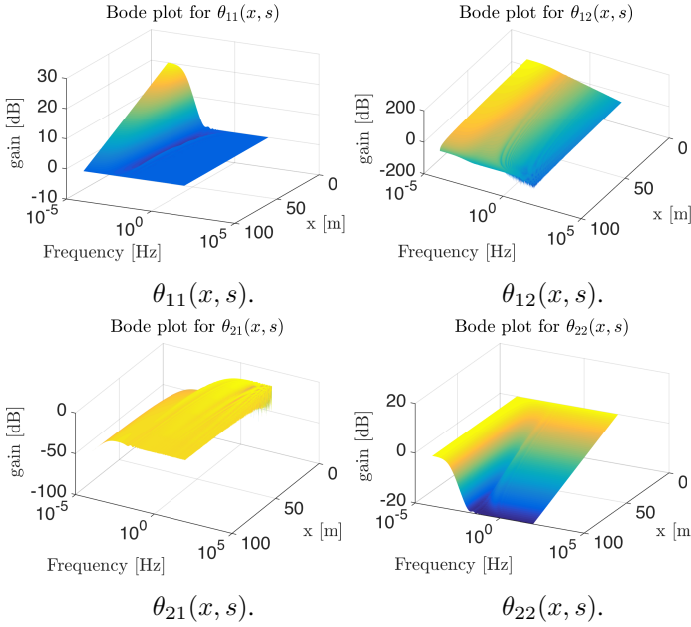


Fig. 4. Spatial magnitude Bode plots for physical variables in congested regime ($|\alpha| = 0.05$ Hz)

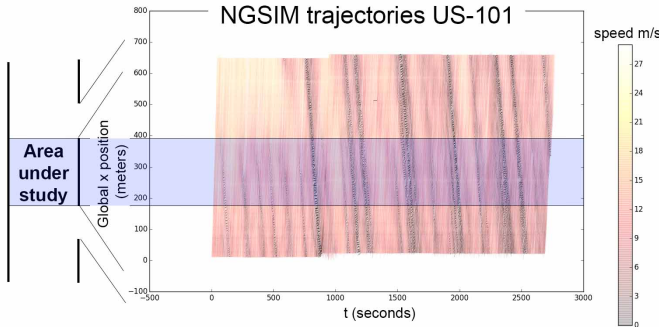


Fig. 5. NGSIM trajectories. Color represents the measured speed of each car in m/s.

have detected poles with a non zero imaginary part, none has been found. Holistic search for other poles should be conducted but is out of the scope of this article.

IV. NUMERICAL VALIDATION

This section compares the prediction of the linearized equations with actual flow and velocity data gathered from the NGSIM data set.

A. Data source: NGSIM trajectories

We use the NSGIM trajectory data set for a uniform 200-meter long section of the US-101 highway where no ramps perturb the homogeneity of traffic. The set gathers 45 minutes worth of trajectories of vehicles sampled with a 10 Hz frequency in the area described in Figure 5.

B. Reconstructing (v, q) maps from NGSIM trajectories

The NGSIM data set does not directly provide the values $v(t, x)$ and $q(t, x)$ in the resolution domain $[0, T] \times [0, L]$. To obtain macroscopic quantities out of the microscopic measurements, we follow the approach devised in [15], dividing

the space-time grid into rectangular cells, grouping corresponding data points into cells and estimating the quantities of interest as done in [16]. The full estimation procedure is described in the appendix attached. We validated this by comparing two vehicular flow estimates obtained by radically different techniques. They both correspond throughout the estimated speed-flow map.

Calibration of λ_1 and λ_2 , linearization point: In Section II, we found that λ_1 is exactly v^* and λ_2 is the slope of the fundamental diagram at v^* . Thus to calibrate the eigenvalues we must find the linearization point. Note the dataset used corresponds only to the congested regime and the fundamental diagram is almost affine. The estimator, $\hat{\lambda}_1 = \hat{v}^*$ is chosen as the empirical mean of \hat{v} . To estimate λ_2 , we fit a linear model $\hat{q} = b_1 \hat{\rho} + b_0 + \varepsilon$ with an ordinary least squares procedure, where ε represents the noise in the model that would ideally be centered, homoschedastic, and uncorrelated but is not practically. Then $\hat{\lambda}_2 = \hat{b}_1$ and we take \hat{q}^* as the empirical average of \hat{q} . The ratio of \hat{q}^* and \hat{v}^* gives the estimate $\hat{\rho}^*$. The empirical results are presented in Figure 6. The determination coefficient is poor but can be improved by filtering out outliers and gathering more data. Further work should turn this rather heuristic method for estimating parameters into a fully justified statistical procedure.

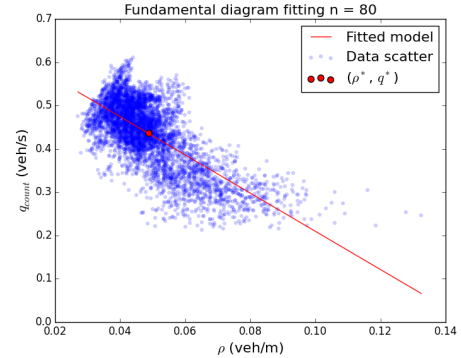


Fig. 6. Calibration of λ_1 and λ_2 . The circle denotes the linearization point. The affine model used to estimate λ_2 and the linearization point is also plotted. The estimates are: $\hat{\lambda}_1 = 8.96$ m/s, $\hat{\lambda}_2 = -4.37$ m/s, $\hat{\rho}^* = 0.049$ veh/m, $\hat{v}^* = 8.96$ m/s, $\hat{q}^* = 0.44$ veh/s, with $r^2 = 0.48$. The characteristic frequency of the system is $\hat{\omega} = 8.37 \times 10^{-3}$ Hz. Its order of magnitude does correspond to practical traffic flow modeling.

Verification of the spectral form: In this section we demonstrate the performance of the spectral form as a prediction tool using the time domain responses derived from the transfer functions above and FFT. Since we are working with a linearized system, we can decompose boundary conditions then add predicted values inside the domain $[0, T] \times [0, L]$. Fourier decomposition of boundary conditions is here extremely accurate as the median relative errors for the interpolation of the values of $\xi_1(x=0, \cdot)$ and $\xi_2(x=L, \cdot)$ are respectively 2% and 3%.

Simulated maps: Since the spectral form presents information in the diagonalized basis, we need a conversion before we can compare the simulated results to the values estimated from the dataset. It takes into account both the fact that the linearized equation are based on deviations of v and

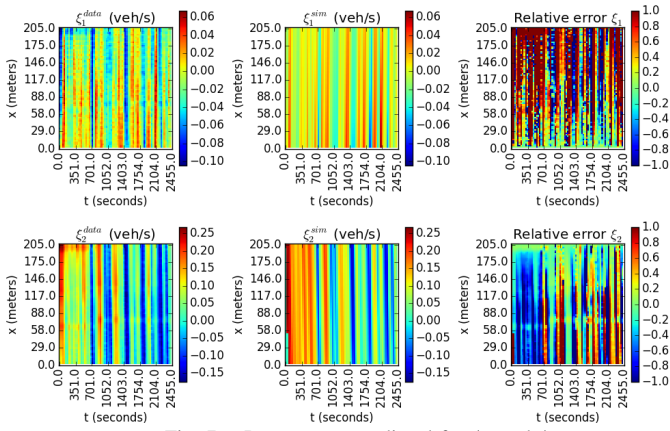


Fig. 7. Data versus predicted for ξ_1 and ξ_2

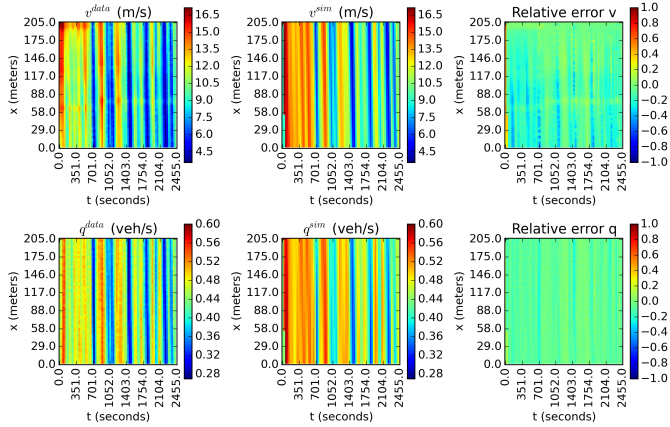


Fig. 8. Data versus predicted for v and q

q from the linearization point and the change of basis that is necessary to work with Riemann invariants. The inverse of this affine transformation yields in return predicted quantities for the physical variables based on the computations of ξ_1 and ξ_2 in the resolution domain.

Figures 7 and 8 shows important qualitative properties of the model. As expected, the model generally predicts with good accuracy the decay of all quantities along their characteristic lines, a realistic feature that cannot be paralleled by first-order models. The general quality of the fit is good with most of the errors on v and q in a 20% range of the data's amplitude between minimum and maximum values, high magnitude errors mostly occur because of noise in the discretized quantities of interest. The linearized second-order model manages to capture oscillations observed on the boundary and account for their decay accurately.

V. CONCLUSION

As the full nonlinear ARZ equations have no known closed form solutions in the general case, they are difficult to analyze. The linearized equations enable the use of spectral methods presented here, allowing for simple yet powerful analysis tools relying on explicit solutions. This approximate model is able to capture important features of the flow which first order models cannot.

With the linearized ARZ model, we were also able to define the Traffic Froude Number F . This quantity is com-

puted using the eigenvalues of the system and characterizes the flow regime of the road section under consideration. The time domain responses we derive show that the system is convectively unstable in free-flow regime ($F < 1$) as opposed to the congested regime case ($F > 1$). In the latter case, the system remains in the linear regime and oscillations on boundary conditions are damped with an exponential rate along the characteristic lines.

Predictions in congested regime for traffic do not present shocks and Fourier spectral analysis cannot account for more nonlinear and non-smooth behavior as well as other transforms such as wavelets. However, our spectral domain study paves the way to applying standard linear system control theory to traffic, with a linearized second order model that is empirically reliable in terms of reproducing actual data. Future work will therefore focus on controller design based on the spectral framework presented here.

ACKNOWLEDGMENTS

The authors wish to thank Dr. Nikolaos Bekiaris-Liberis, Pierre-Olivier Lamare (PhD student at laboratoire Jean Kuntzmann) and Dr. Guillaume Costeseque for their support.

REFERENCES

- [1] B. A. Zielke, R. L. Bertini, and M. Treiber, "Empirical measurement of freeway oscillation characteristics: an international comparison," *Transportation Research Record: Journal of the Transportation Research Board*, vol. 2088, no. 1, pp. 57–67, 2008.
- [2] Y. Sugiyama, M. Fukui, M. Kikuchi, K. Hasebe, A. Nakayama, K. Nishinari, S. ichi Tadaki, and S. Yukawa, "Traffic jams without bottlenecks, experimental evidence for the physical mechanism of the formation of a jam," *New J. Phys.*, vol. 10, p. 033001, 2008.
- [3] H. J. Payne, *Models of Freeway Traffic and Control*. Simulation Councils, Incorporated, 1971.
- [4] G. B. Whitham, *Linear and Nonlinear Waves*. Wiley, 1974.
- [5] M. J. Lighthill and J. B. Whitham, "On kinematic waves. II: A theory of traffic flow on long crowded roads," *Proc. Royal. Soc.*, pp. 317–345, 1955.
- [6] P. I. Richards, "Shock waves on the highway," *Operations Research*, vol. 4, no. 1, pp. 42–51, 1956.
- [7] C. F. Daganzo, "Requiem for second-order fluid approximations of traffic flow," *Transp. Res. B*, vol. 29, no. 4, pp. 277–286, 1995.
- [8] A. Aw and M. Rascle, "Resurrection of second order models of traffic flow," *SIAM Journal of Applied Mathematics*, vol. 60, no. 3, pp. 916–938, 2000.
- [9] R. M. Colombo, "Hyperbolic phase transitions in traffic flow," *SIAM Journal on Applied Mathematics*, vol. 63, no. 2, pp. 708–721, 2003.
- [10] S. Fan, M. Herty, and B. Seibold, "Comparative model accuracy of a data-fitted generalized Aw–Rascle–Zhang model," *Networks and Heterogeneous Media*, vol. 9, no. 2, pp. 239–268, 2014.
- [11] X. Litrico and V. Fromion, *Modeling and control of hydrosystems*. Springer, 2009.
- [12] T. W. Sturm, *Open channel hydraulics*. McGraw-Hill, 2001.
- [13] A. Hoffeitzer, C. Claudel, and A. Bayen, "Reconstruction of boundary conditions from internal conditions using viability theory," in *American Control Conference*, pp. 640–645, IEEE, June 2012.
- [14] B. S. Kerner and H. Rehborn, "Experimental properties of phase transitions in traffic flow," *Phys. Rev. Lett.*, vol. 79, pp. 4030–4033, Nov 1997.
- [15] L. C. Edie, "Discussion of traffic stream measurements and definitions," in *Proc. 2nd Int. Symp. on the Theory of Traffic Flow*, pp. 139–154, 1963.
- [16] B. Piccoli, K. Han, T. L. Friesz, T. Yao, and J. Tang, "Second-order models and traffic data from mobile sensors," *Transp. Res. C*, vol. 52, pp. 32–56, 2015.